Recovery of Point Source Flux Density and Position from SPIRE POF 2 Observations

Bruce Sibthorpe, Tim Waskett, Matt Griffin

DOCUMENT No.: SPIRE-UCF-NOT-002315

Issue 1.0

Date: 4 July 2005

Abstract

This note outlines an investigation into the effects of pointing error, signal to noise ratio, and grid spacing on a SPIRE POF 2 observation, and how their effects influence our ability to recover the original source position and flux density from the derived data. The investigation was carried out using the SPIRE Photometer Simulator v1.0 and data reduced using two simple in house 2D Gaussian fitting routines. The telescope beam was assumed to be symmetric.

Results showed that for high SNR and low pointing error, i.e. a pointing calibration observation, the 1σ error in source position and flux density is ~3% of a beam, and ~4% respectively. These values increased to 25% and 27% respectively for poor SNR (~3) and pointing (~0.5 beam). The optimum grid spacing was found to be ~0.3 beam, which corresponds to ~5" (PSW band).

Contents

1. Introduction

This note presents the results of an investigation of the uncertainties involved in the determination of flux density and position from small map observations of point sources with SPIRE using the POF 2 or a similar observing mode. POF 2 (B. M. Swinyard and M. J. Griffin 2002) is defined as a seven-point observation; here we analyse, for computational convenience, the case of a nine-point square grid. The main conclusions will also apply to the case of a seven-point.

The impact of pointing error (Δ), signal to noise ratio (SNR), and map grid spacing (θ) on the recovery a source's flux density and position have been assessed by a statistical analysis of a large number of observations with random errors. The results indicate the measurement quality that may be expected in various circumstances, and provide a quantitative basis for the choice of the optimum map grid spacing.

2. Photometer Observatory Function 2 (POF 2)

There are two potential sources of pointing error when carrying out a POF 2 observation, the telescope absolute pointing error (APE), and any error in a source's catalogued astrometric position. Pointing error when quoted within this investigation should be regarded as the sum of the two errors.

The Herschel APE goal is given by a 1σ pointing error of 3.7". This, in addition to possible errors in known source position, leads to a potential positional error of ~6". Given the SPIRE FWHM beam sizes of ~17, 24 and 34", this equates to errors of ~0.35, 0.25 and 0.18 beams respectively.

The SPIRE POF 2 observing mode is foreseen to be adopted to estimate simultaneously the flux density and position of a point source. It will be carried out by performing seven individual chopped observations, as shown in Figure 2a, to generate a small map of the source and the surrounding region. A 2D Gaussian can then be fit to these data returning both the source's flux density and position with respect to the central pointing.

This observatory function requires no movement of the telescope – the beam position is adjusted and modulated via the beam steering mirror (BSM).

3. POF 2 simulations

A nine-point map was used to carry out this investigation (as shown in Figure 2b) as this approach is computationally simpler and its results are equally applicable to the seven-point map case (Figure 2a).

The investigation was carried out using data produced by the SPIRE Photometer Simulator (SPSv1.0) (Sibthorpe et al. 2004). White noise was added to a 'clean' bolometer voltage timeline with a noise voltage spectral density equal to that derived from the simulator bolometer module. White noise is appropriate in this case as this is a chopped observation, and not significantly affected by $1/f$. For each chosen parameter set, 1000 runs, each utilising a unique noise timeline, were carried out in order to achieve a statistically significant data set.

The effect of pointing error was examined by adjustment of the source position with respect to the telescope bore-sight. The source was positioned at various points along the y-axis. In principle this is sufficient as the variation in total SNR as a function of pointing error direction is negligible, as shown in Figure 1. To ensure this was in practice the case three tests were carried out varying the pointing error direction while keeping all other parameters constant (θ = 0.35, Δ = 0.25, SNR_{peak} ~ 30). These tests showed a maximum variation of ~1% in flux recovery and 0.1% in positional recovery. Such values are negligible in comparison with the effects of the parameters being investigated.

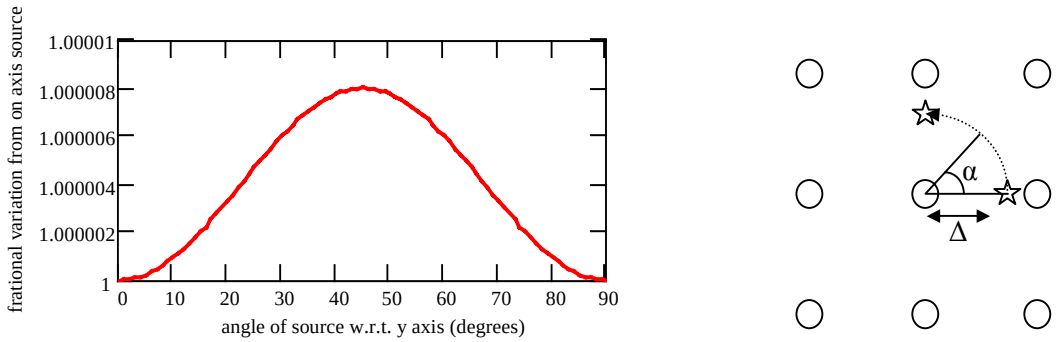

Figure 1: Variation in total signal to noise loss factor as a function of source positional rotation about the central map chop position (α), with fixed pointing error (Δ = 0.1 beam). Map size, θ = 0.3 beam

The PSW band was taken as the test case and explicit values of the parameters were chosen to provide appropriate coverage of the parameter space, but the results have been normalised in terms of the beam width so as to make them generally applicable.

Telescope and BSM pointing jitter or drift were assumed to be negligible during the observations.

The beam profile was taken to be a Gaussian, and an important assumption is that the beam profile is perfectly symmetrical. Although this is not important for the case of low or modest signal-to-noise observations, in which case small departures from beam symmetry are masked by statistical errors, in the case of high signal-to-noise, the recovery of the position is critically dependent on an accurate knowledge of the beam profile.

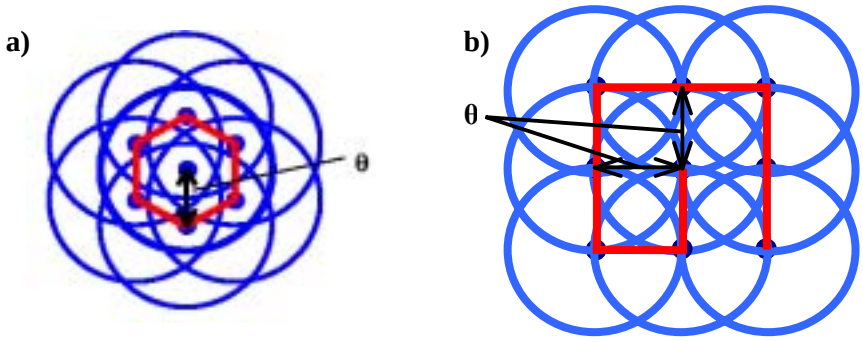

Figure 2: a) Seven-point jiggle map; b) nine-point jiggle map

3.1 Adopted parameters

Table 1 summarises the main parameters adopted in the simulations.

Simulator set-up	
Tests carried out using PSW waveband	Results normalised to beam
Time sampling step size within simulation	12.0 ms (→ 83.3 Hz)
Sky	
Size	1000 x 1000 pixels
Resolution (pixel size)	2 arcsec / pixel
Source position	Pixel (500, 500)
Source flux density	30, 60, 100, 300, 600, 1000 mJy
Corresponding associated peak SNR	~ 2.8, 5.6, 9.4, 28.1 56.1, 93.5
Optics	
Simple Gaussian beams	

Full optical chain	
'Top-hat' filters	
POF2	
Chop throw	126 arcsec
Integration per position	10.08 s (i.e. 20 chops per position)
Chop frequency	~ 2.08 Hz
Chop direction	along y axis (S/C coordinates)
θ – as defined in figure 2	4, 6, 8,10 arcsec
- normalised to beam FWHM	0.24, 0.35, 0.47, 0.59 beam
Detectors	
3 detectors, 1 per waveband	
Operation in linear regime	
Detector sampling rate	27.7 Hz (→ 36.0 ms)
Noise	
Telescope pointing jitter	Negligible, not implemented
Pointing error (APE) + astrometric error	0, 2, 4, 6, 8 arcsec
- normalised to beam	0, 0.12, 0.23, 0.35, 0.47 beam
White noise level as derived within bolometer module (noise level due to the bolometer and background photon noise)	$e_n = 28\ nVHz^{-½}$

Table 1: Simulation parameters

3.2 Data analysis methods

Two different 2-D Gaussian fitting routines were used. One used an analytical method applied to various one-dimensional cuts in the map, initially estimating the source position, and then using this position to determine the source flux density (height of the Gaussian). The second used a least squares fit to all of the data to recover both flux density and position simultaneously (see Appendix I for details).

Statistical analysis of data from 1000 runs was carried out. The positional uncertainty was characterised by the population RMS in the difference between the actual and estimated positions, normalised to the beam FWHM. The positional uncertainties correspond to the radial offset from the actual position (i.e., the quadrature combination of the errors in the two coordinates). While there is no pointing error in the z direction, recovery of the source in this axes is still subject to noise effects, hence it is included. The flux density uncertainty was calculated as the population RMS normalised to flux density, (i.e., the 1-σ fractional error in the recovered flux density).

4. Results

In order to illustrate the main conclusions, we present here the results for simulations based on two nominal cases as indicated in Table 2.

(i) a favourable case: Zero pointing error, good peak SNR (~ 10), grid spacing chosen for best compromise between overall SNR and ability to cope with large pointing error;
(i) an unfavourable case: Large pointing error, poor peak SNR (~ 3), non-optimal grid spacing.

Based on these two nominal cases, results are presented below which cover wide ranges of the three parameters.

	Favourable Case	**Unfavourable Case**
Pointing error Δ / beam FWHM	0	0.47
Grid spacing θ / beam FWHM	0.35	0.23
Peak signal to noise ratio SNR_{peak}	~ 10	~ 2.8

Table 2: Sample observing situations

Note: The peak signal to noise ratio, SNR_{peak}, is defined as the signal to noise ratio that would be achieved at the central chop position with zero pointing error. This definition of the SNR parameter is required as the total SNR for an observation is also a function of both map spacing and pointing error.

All graphs plotted below display either uncertainty in position or flux density recovery as a function of one of the three parameters (Δ, θ, SNR_{peak}). For each parameter there are two pairs of graphs, displaying a family of curves for one parameter with the remaining free parameter held constant at its extreme values as defined in Table 2.

4.1 Flux density and position recovery vs. SNR_{peak} for various values of pointing error

Figure 3 shows the statistically-derived fractional uncertainty in the recovered flux density as a function of SNR_{peak} for various values of the pointing error. The left panel is for the case of a grid spacing of 0.35 beam and the right for 0.23 beam. Figure 4 shows the uncertainty in the recovered position (normalised to the beam FWHM) for the same conditions.

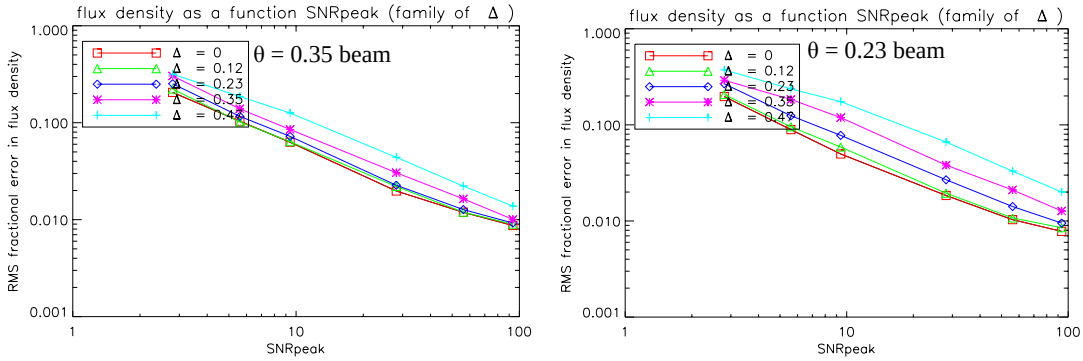

Figure 3: Uncertainty in source flux density recovery as a function of SNR in the favourable (left) and unfavourable (right) cases for a variety of pointing error values.

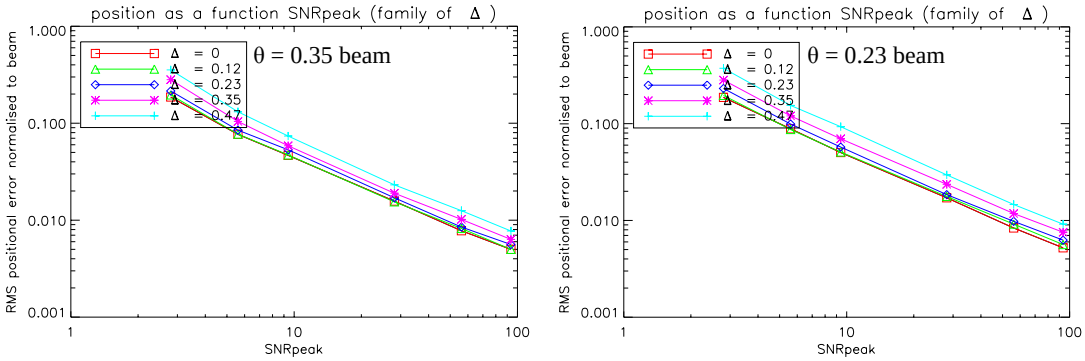

Figure 4: Uncertainty in source position recovery as a function of pointing error in the favourable (left) and unfavourable (right) cases for a variety of pointing error values.

From Figure 3, we see that for zero pointing error, the flux density is recovered to an accuracy somewhat better than the value of SNR_{peak} (due to the co-addition of the nine points in the map). For a pointing error of 0.35 beam, the final SNR is about equal to SNR_{peak}. The lower grid spacing of 0.23 beams provides somewhat better performance if the pointing error is small, but worse in the case of large pointing errors. The optimum choice of θ thus depends on the expected magnitude of the typical pointing errors.

Figure 4 shows that for low pointing error and high SNR_{peak}, the fractional error in the recovered position is slightly better than the value of SNR_{peak} (e.g., for SNR_{peak} = 100, we have about 0.8% of a beam uncertainty in position).

As a rule of thumb, we conclude that both the signal and position can be recovered to an accuracy comparable to SNR_{peak}.

In considering the case of high SNR, it is important to remember that we are assuming a symmetrical beam. Any departure from symmetry that is not known to high accuracy will introduce a comparable uncertainty. So if the beam is asymmetrical at the 2% level, and this is not explicitly taken into account in the fitting, then this will introduce a corresponding error in the recovered position. Likewise, other sources of error which we have neglected here could become influential in the case of observations made with high instantaneous SNR, such as telescope or BSM pointing jitter, detector responsivity drift, etc.). We assume that the most accurate measurement of the pointing offsets that will be feasible with SPIRE is about 3% of the beam FWHM. In the case of the smallest beam (PSW, 18") his corresponds to approximately 0.5". Achieving such accuracy will require careful and dedicated measurements. Such measurements are envisaged as part of the process of refining and improving the satellite pointing model.

It should be noted that the results do contain some oddities in the extreme cases. At low SNR, fit to these data is extremely difficult, thus the accuracy determined is influenced by the fitting routine. At high SNR the fitting routine used here is limited by the finite grid resolution for high SNR cases.

4.2 Flux density and position recovery vs. SNR_{peak} for various values of grid spacing

Figure 4 shows the fractional uncertainty in the recovered flux density as a function of SNR_{peak} for various values of the grid spacing and for two extreme values of pointing error: zero (left) and 0.47 beam (right). Figure 5 shows the uncertainty in the recovered position (normalised to the beam FWHM) for the same conditions.

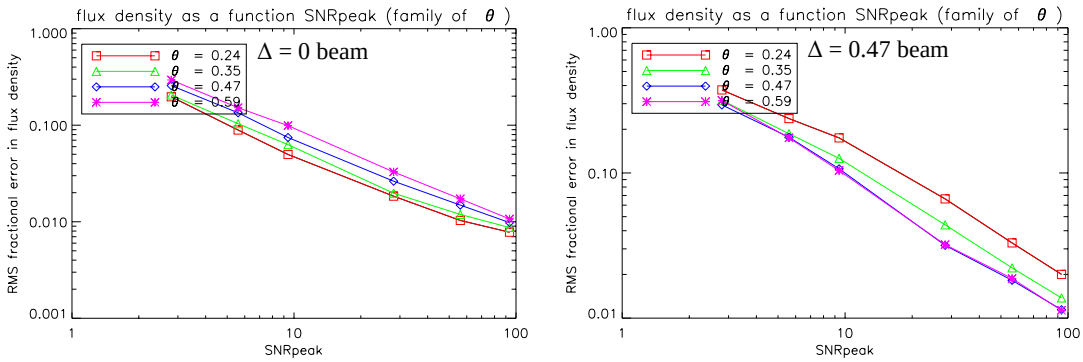

Figure 4: Uncertainty in source flux density recovery as a function of SNR in the favourable (left) and unfavourable (right) cases for a variety of grid spacing values.

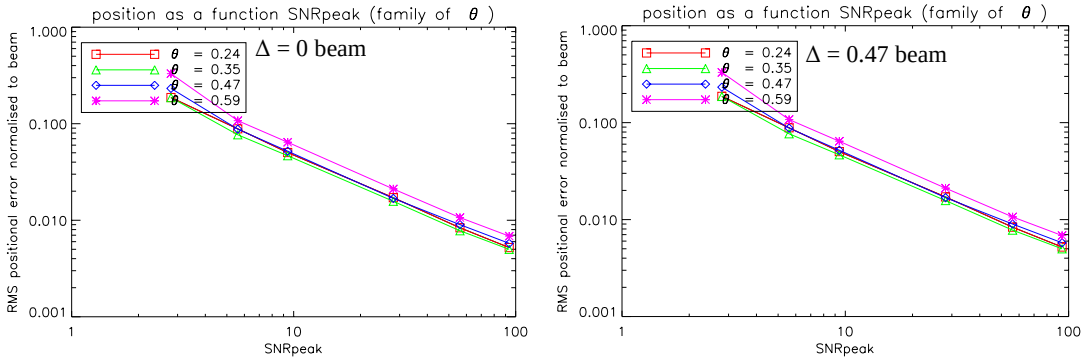

Figure 5: Uncertainty in source position recovery as a function of SNR in the favourable (left) and unfavourable (right) cases for a variety of grid spacing values.

Figure 5 (left) shows that for small pointing error, the optimum grid spacing is small (as it provides maximum signal in all the map points without compromising the pointing accuracy). The right hand panel indicated that even for large pointing error, a small grid spacing is still appropriate (with $\theta = 0.24$ and 0.35 producing comparable results).

We can conclude from Figure 5 that for grid spacings up to about 0.5 beam, the recovery of position is also much the same. However, the logarithmic scale in these figures makes it difficult to discern small

differences - in Section 4.3, a more accurate characterisation of the optimum grid spacing is presented and discussed.

4.3 Flux density and position recovery vs. pointing error for various values SNR_{peak}

Figure 6 shows the fractional uncertainty in the recovered flux density as a function of normalised pointing error for various values of SNR_{peak} for values of grid spacing: 0.35 beam (left) and 0.23 beam (right). Figure 7 shows the uncertainty in the recovered position (normalised to the beam FWHM) for the same conditions.

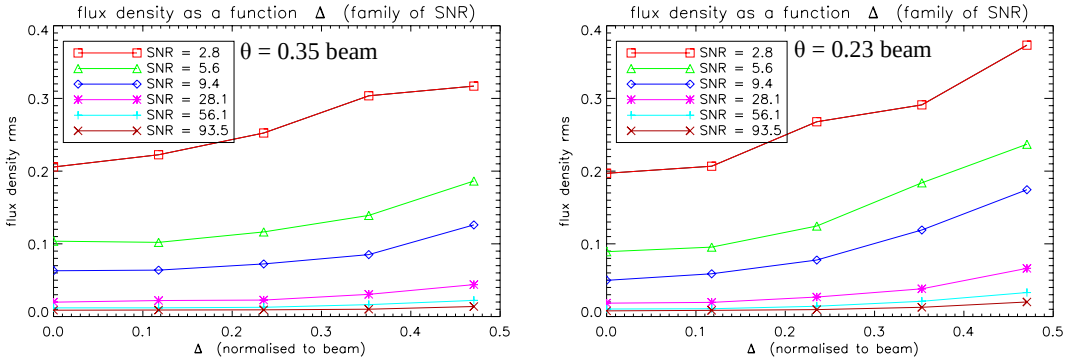

Figure 6: Uncertainty in source flux density recovery as a function of pointing error in the favourable (left) and unfavourable (right) cases for a variety of SNR values.

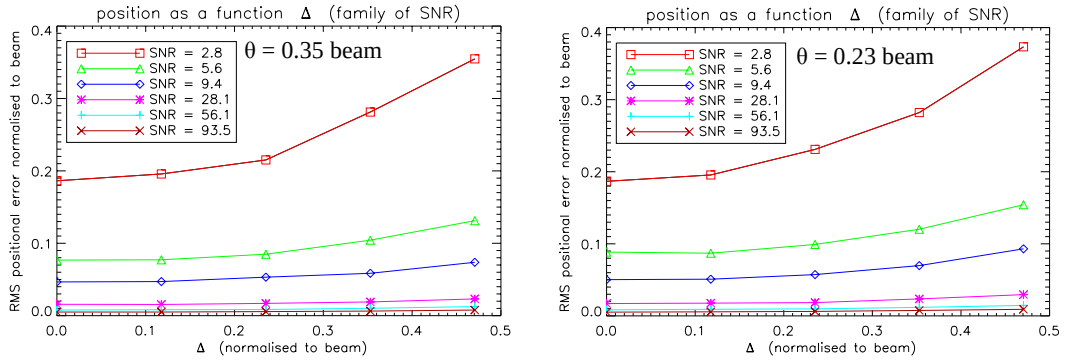

Figure 7: Uncertainty in source position recovery as a function of pointing error in the favourable (left) and unfavourable (right) cases for a variety of SNR values.

From Figure 7, we note that, as expected, there is a decrease in signal accuracy with increasing pointing error. For the two adopted map spacings the results are only slightly different. For modest SNR_{peak} (~ 10), a value of $\theta = 0.35$ provides good performance over a wide range of pointing errors. The smaller grid spacing is a bit better for accurate pointing but rather worse for the case of poor pointing accuracy.

A slight kink can be seen in both graphs at a SNR_{peak} level of 2.8 at the points where the grid spacing is the same as the pointing error. This is a result of the source passing across the adjacent map position. The last value for the $\theta = 0.35$ beam case can be seen to be unexpectedly low. This increased accuracy occurs due to the high SNR achieved at the nearby map position. The same can be seen in the other case where here the grid spacing is 0.23 beam. The point immediately following the exit of the source from the map is again unexpectedly low, however the subsequent point resumes the decrease in accuracy and turns up again as the source moves further from the map.

The influence of grid spacing on the measurement quality is considered in more detail in the next section.

4.4 Flux density and position recovery vs. pointing error for various values SNR_{peak}

Figure 8 shows the fractional uncertainty in the recovered flux density as a function of normalised pointing error for various values of grid spacing and for two values of SNR_{peak}: ~10 (left) and ~ 3 (right).

Figure 9 shows the decrease in positional accuracy with increasing pointing error, and demonstrates the small impact of the grid size parameter, seen by the small variation in both cases. For SNR_{peak} ~ 10 and θ = 0.35, the position is recovered with an uncertainty of about 5%.

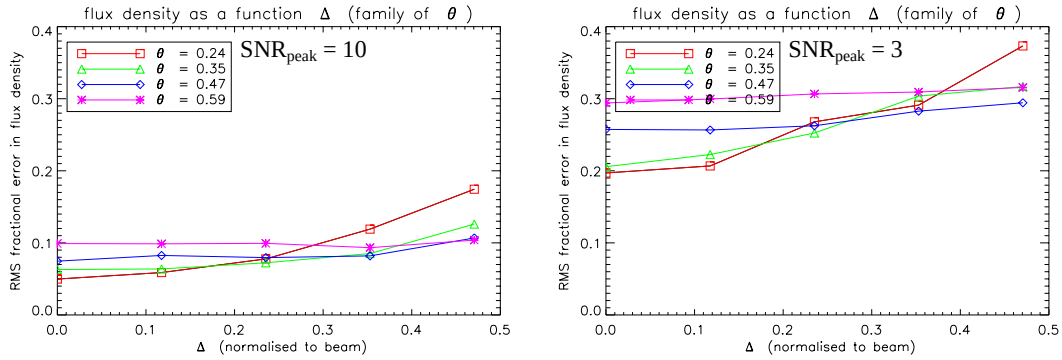

Figure 8: Uncertainty in source flux density recovery as a function of pointing error in the favourable (left) and unfavourable (right) cases for a variety of pointing error values.

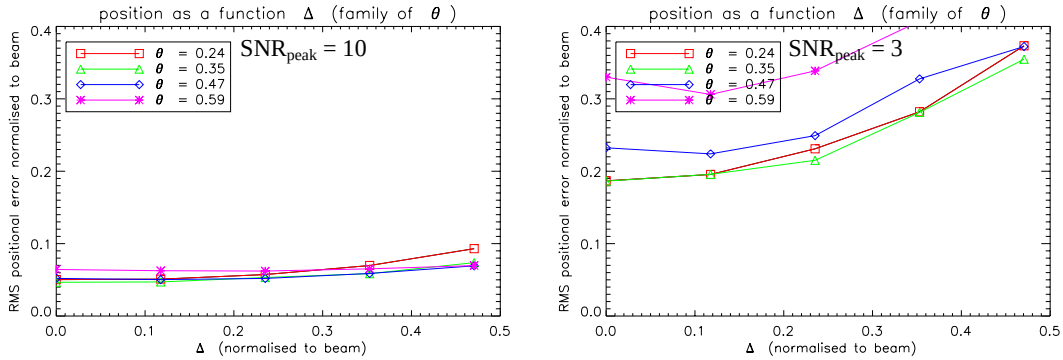

Figure 9: Uncertainty in source position recovery as a function of pointing error in the favourable (left) and unfavourable (right) cases for a variety of pointing error values.

Figure 8 illustrates a slight upturn with increasing pointing error (~0.47 beam) but is on the whole reasonably flat. Once the source has passed outside the gird, the accuracy of the fit degrades more quickly; hence while the smaller grid spacing maps have a higher initial accuracy, they are more susceptible to pointing errors, while the effect on larger maps is less significant. This can be seen in both graphs in Figure 8 by the cross-over of the data at approximately $\theta = \Delta$. For the case of good SNR (left panel), a grid spacing of 0.35 beam provides a good compromise between sensitivity and ability to cope with large pointing error.

For the higher SNR_{peak} case (Figure 9, left), the uncertainty in recovered position is very weakly dependent on the grid spacing. Again, a peak SNR of about 10 gives ~ 5% uncertainty for a wide range of pointing errors. For the low SNR case, the error in position is correspondingly low, and increases significantly for large pointing error where the combination of poor SNR and inaccurate pointing results in a poor quality measurement.

4.5 Flux density and position recovery vs. pointing error for various values SNR_{peak}

Figure 10 shows the fractional uncertainty in the recovered flux density as a function of normalised grid spacing for various values of SNR_{peak} and for two values of pointing error: 0 (left) and ~ 0.47 beam (right). Figure 11 shows the uncertainty in the recovered position for the same conditions.

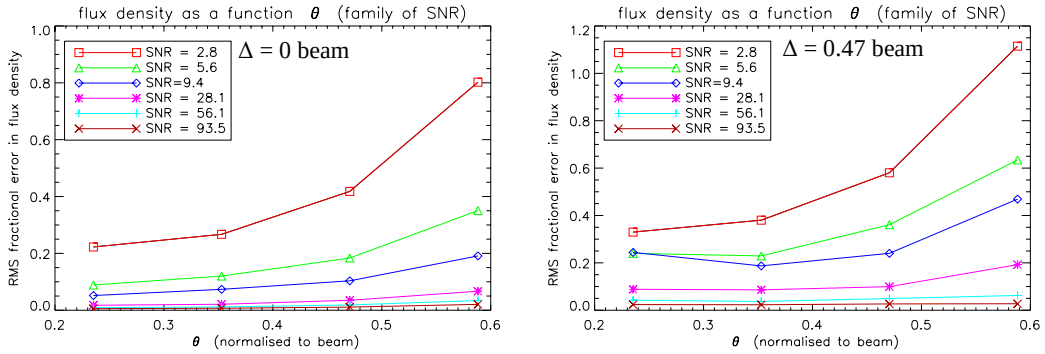

Figure 10: Uncertainty in source flux density recovery as a function of grid spacing in the favourable (left) and unfavourable (right) cases for a variety of SNR values.

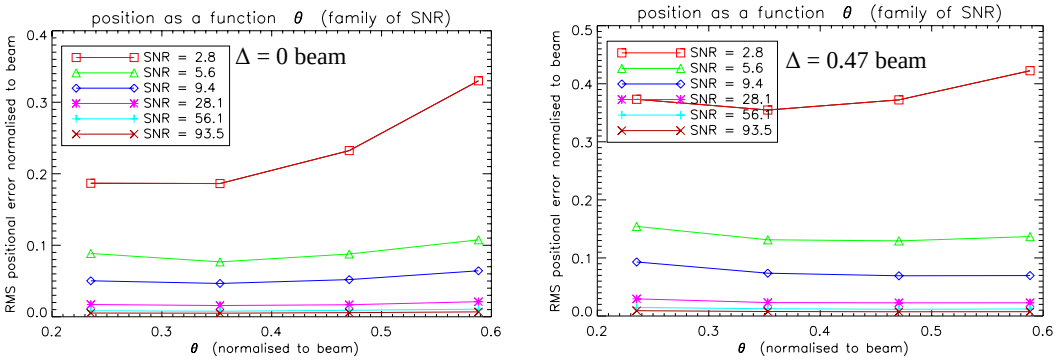

Figure 11: Uncertainty in source position recovery as a function of grid spacing in the favourable (left) and unfavourable (right) cases for a variety of SNR values.

The variation seen in Figure 10 is as predicted by theory (Griffin et al. 2002) for the case of zero pointing error, i.e. an increasing error with grid spacing.

As seen before, Figure 10 shows how for low pointing error, the overall SNR on the recovered signal is somewhat better than SNR_{peak} due to the co-addition of the nine map points, and in the case of large pointing error, the overall SNR of the measured flux density is much lower than what would be obtained with accurate pointing. Even for large pointing error, a small grid spacing still produces the best results, with an optimum values of about 0.35 for the case of $SNR_{peak} = 10$.

Figure 11 also shows that the in the case of large pointing error, the flux density measurement accuracy is optimised when the map grid spacing is suitably chosen. This minimum occurs because there is a greater contrast in the signal obtained from the various chop positions at higher grid spacing, thereby allowing the fit routine to operate more accurately. In cases of low SNR however this difference is negligible and therefore is not visible in the unfavourable-case data.

For small pointing error, and small grid spacing (Figure 11, left), the fractional error in the recovered position is 2-3 times better than SNR_{peak}. This holds even for large grid spacing provided that SNR_{peak} is not too small. As noted above, this case of small pointing error and high SNR is an important one: it corresponds to an attempt to determine the pointing offsets to the highest possible accuracy by observing a bright source of accurately known position with an initial estimate of the offsets that is already fairly accurate.

4.6 Flux density and position recovery vs. grid spacing for various values of the pointing error

Figure 13 shows the fractional uncertainty in the recovered flux density as a function of normalised grid spacing for various values of pointing error and for two values of SNR_{peak}: ~ 10 (left) and ~ 3 (right). Figure 14 shows the uncertainty in the recovered position for the same conditions.

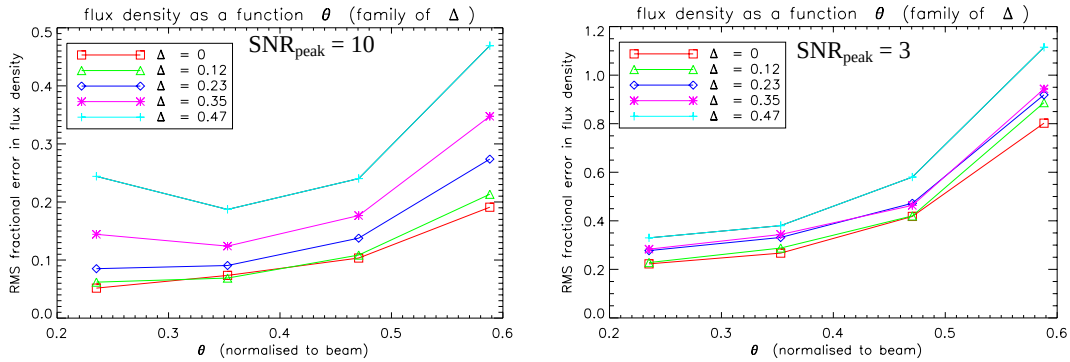

Figure 13: Uncertainty in source flux density recovery as a function of grid spacing in the favourable (left) and unfavourable (right) cases for a variety of pointing errors values.

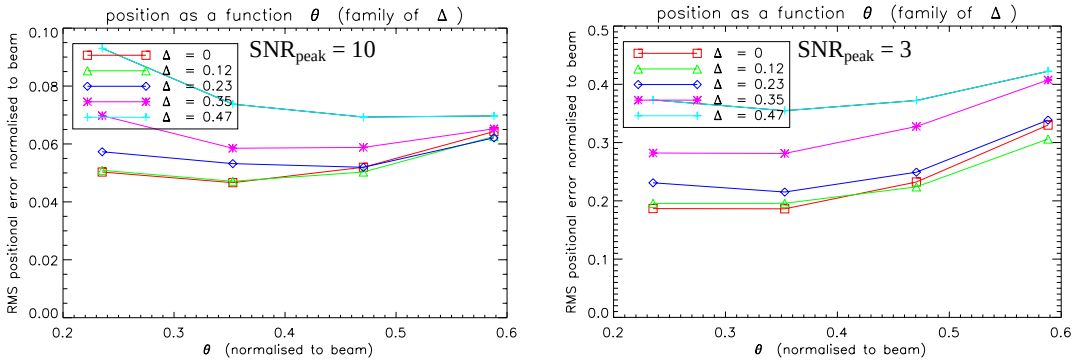

Figure 14: Uncertainty in source position recovery as a function of grid spacing in the favourable (left) and unfavourable (right) cases for a variety of pointing errors values.

Figure 13 shows a clear optimum when θ is equal to or slightly less than Δ. This benefit occurs up until a point at which the decrease in overall SNR resulting from a larger map begins to dominate over the improvement of fit.

Figure 14 reveals that larger maps are less affected by pointing errors. For a modest SNR_{peak} of ~ 10, the optimum spacing is about 0.35 beam for pointing error less than 0.35 beam, but a larger map would appropriate for the case of less accurate pointing. In a situation with low SNR and good pointing error however, a large map would be significantly sub-optimal.

5. Conclusions

To summarise the main conclusions of this analysis, we consider some representative cases

- High SNR; low pointing error:
  - Corresponds to pointing calibration observation
  - Recovery of flux density and position to an accuracy comparable to SNR_{peak}
  - Highly accurate recovery of position depends critically on beam symmetry and negligible distortion due to other systematic effects.
  - To allow for some degradation in performance due to other effects, we assume that the highest quality measurement of position that will be practical is about 3% of the smallest (PSW) FWHM, corresponding to about 0.5".

- Modest SNR (~10); modest pointing error (~ 0.2-0.3 beam = 3.5 – 5.5")
  - Corresponds to observing a typical point source observation with APE plus maybe a small uncertainty in the source position
  - Optimum grid spacing is about 0.3 beam (This size suits all bands, despite the variation in beam sizes, as a high pointing error is still relatively small as a fraction of the larger beam sizes. This

would also allow the longer wavelength bands to benefit from the advantages seen when using a smaller map)
    - Source position with error ~ 7% of a beam, and a flux density error ~ 7%.

- Poor SNR (~ 3); modest pointing error (~ 0.2-0.3 beam = 3.5 – 5.5")
    - Not likely to occur very often as confusion will come into play after an integration of about 15 minutes.
    - Grid spacing of 0.3 beam still OK
    - Source position with error ~ 25% of a beam, and a flux density error ~ 27%.

Results from both fitting routines were overall in agreement, with differences only occurring at the extremes of the data set. These differences are the result of the individual limitations of the fitting routines (see Appendix). The data sets above contain data from both routines, with the data selected as applicable to the parameters used, e.g. high SNR measurements used data derived via an analytic fit, while low SNR measurements used the least squares method.

6. References

B. Sibthorpe, A. Woodcraft, M. Griffin, S. L. Watkin, A *software simulator for the Herschel-SPIRE imaging photometer*, Proc. SPIE 5847 , Glasgow 21-25 June 2004.
B. M. Swinyard and M. J. Griffin, *Operating Modes for the SPIRE Instrument. SPIRE-RALPRJ-000320*, January 2002.
M. J. Griffin, J. J. Bock, W. K. Gear, *Relative performance of filled and feedhorn-coupled focal-plane architectures,* Applied Optics, 41, 31, 2002

7. Glossary

Beam – telescope beam size as defined by the FWHM, used for normalisation of results
SNR_{total} – Sum of SNR at each chop position
SNR_{peak} – SNR that would be achieved at the central chop position in the presence of zero pointing error.
FWHM – Telescope full width half maximum
SNR – Signal to noise ratio
BSM – Beam steering mirror
POF – Photometer observing function (POF 2 – 7 point jiggle map)

8. Appendix

The two fitting routines used in the reduction of these data are described below.

8.1 Analytic fitting method

This method initially finds the source position, and subsequently uses this position to determine the source flux density (height of the Gaussian).

Simultaneous equations are used to eliminate the unknown height parameter using two points on a fixed line across the chop position grid:

$$a = \frac{2\sigma \ln\left(\frac{f(x_1)}{f(x_2)}\right) + x_1^{\,2} - x_2^{\,2}}{2(x_1 - x_3)}, \qquad \textbf{eq. 1}$$

where a is the central position of the Gaussian, σ is the known standard deviation of the Gaussian (derived from beam FWHM), and $f(x)$ is the datum at position point x_i.

Using the equation above, each slice across the map will return three estimates of the centre of the Gaussian (two points are needed to provide an estimate producing, via combinations, three results per line), giving 9 estimates in total. The final value for the position of the Gaussian on that axis is then the mean of these values. This made use of the total data set. Position in the counterpart axis was then determined using the same method with appropriate combinations of points.

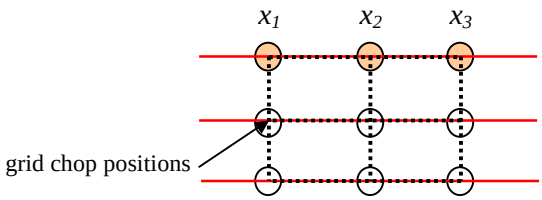

$$a(x_1, x_2) \rightarrow a_{12}$$
$$a(x_1, x_3) \rightarrow a_{13}$$
$$a(x_2, x_3) \rightarrow a_{23}$$
$$\vdots$$

Using this derived position, the peak value for the Gaussian is found using,

$$S = \frac{\sum_{i=0}^{n} \frac{f(x_i, y_i)}{\exp\left(\frac{-(x_i - a) - (y_i - b)}{2\sigma^2}\right)}}{n}, \qquad \textbf{eq. 2}$$

where S is the height of the 2D Gaussian, $f(x_i,y_i)$ is the datum at position i, and n is the number of points in the map.

This method is subject to spikes in flux density in instances of high positional error. This occurs as the flux determination uses the source position found previously. Any positional error has an exponential result on the returned flux, as shown by equation 2. Taking an RMS value from a histogram of these data filtered these spikes.

8.2 Least squares method

The least squares method fits both the height and position of a 2D Gaussian simultaneously. It uses three levels of grid to fit the Gaussian, starting with a large area coarse grid search followed by two smaller searches with increasing resolution.

This method suffers from resolution effects in high SNR cases and a large number of spikes are seen in the derived value for the height of the Gaussian at low SNR and high pointing error. These spikes are due to the routine fitting to local minima.